Supporting Information

Simultaneous Formation of FeO_x Electrocatalyst Coating within Hematite Photoanodes for Solar Water Splitting

Dominic Walsh,[*†] *Jifang Zhang,*[†] *Miriam Regue,* [§†] *Ruchi Dassanayake*[†] *and Salvador Eslava**[†]

[†]Dept. of Chemical Engineering, University of Bath, Claverton Down, Bath, BA2 7AY, UK.

[§] Centre for Sustainable Chemical Technologies, University of Bath, Claverton Down, Bath, BA2 7AY, UK

* Email: d.walsh2@bath.ac.uk; s.eslava@bath.ac.uk

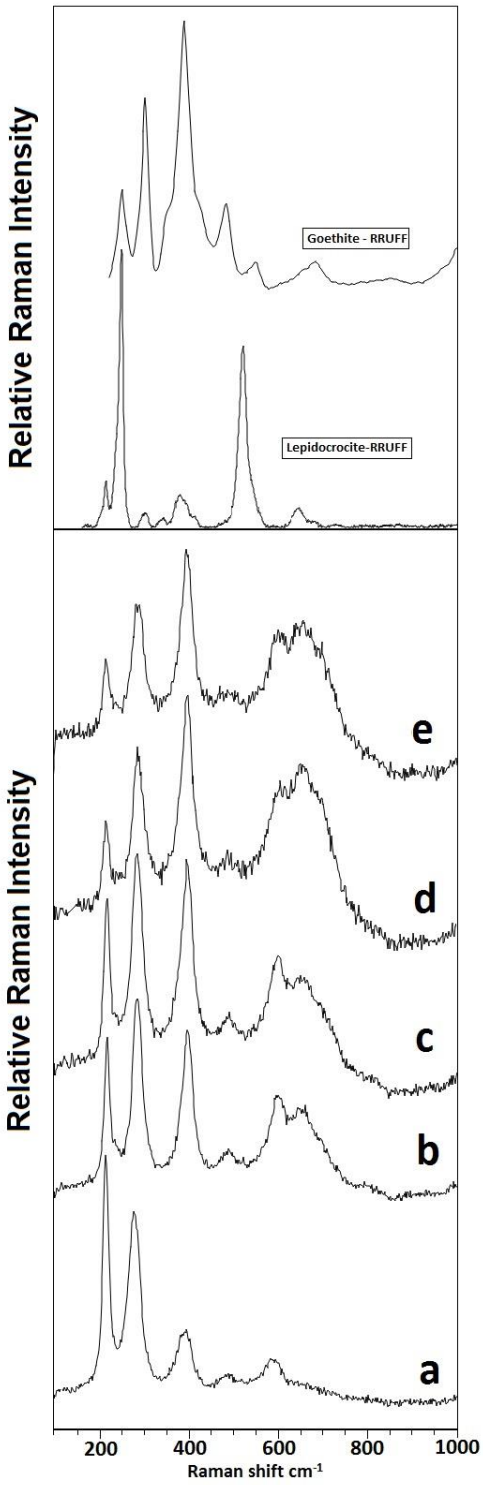

Figure S1. Raman spectroscopy collected using 532nm laser source of FeOOH powders prepared with different levels of LA. (a) 0g LA; (b) 0.1g LA; (c) 0.2g LA; (d) 0.3g LA; (e) 0.4g LA. For comparison, two 532nm Raman spectra of known samples of (unoriented) goethite (α-FeOOH) and lepidocrocite (γ-FeOOH) from the RRUFF mineral database are also shown above.

Table S1. Band positions (cm^{-1}) and relative intensities (in parenthesis: w = weak, m = medium, s = strong, vs = very strong) for the most significant bands in the Raman spectra of prepared FeOOH powders. Raman bands of γ-FeOOH and α-FeOOH from the RRUFF database and a β-FeOOH (schwertmannite) phase are shown for comparison.[1,2]

Sample	Relative Raman Intensity					
γ-FeOOH (0g LA)	214(s)	275(s)	394(m)	487(w)	585(w)	
γ/α -FeOOH (0.1-0.4g LA)	217(s)	290(s)	400(vs)	480(m)	600(s)	660(s)
γ -FeOOH (RRUFF)	216(w)	250(vs)	396(s)		525(s)	650(w)
α -FeOOH (RRUFF)		250(m)	302(s)	484(m)	550(w)	684(w)
'β-FeOOH like'[2]	212(s)	278(m)	390(w)	477(w)	587(w)	

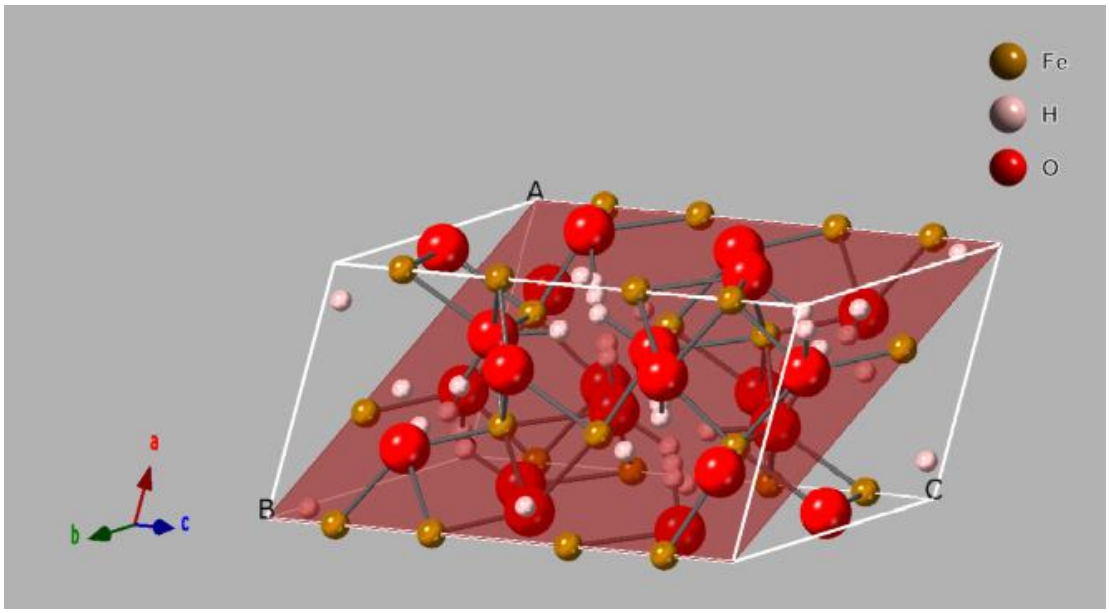

Figure S2. Crystallographic diagram of α-Fe_2O_3 hematite showing iron rich (110) plane.

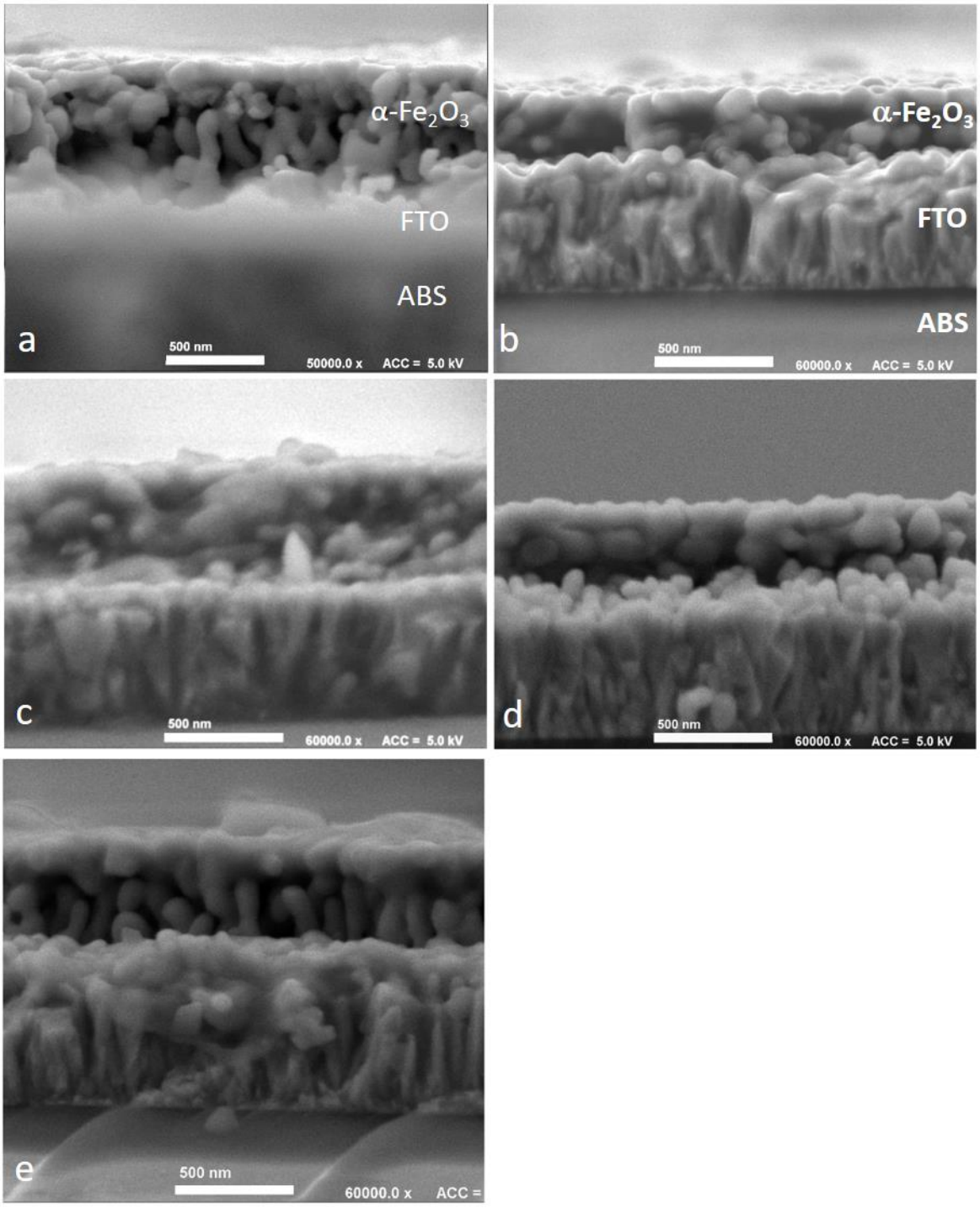

Figure S3. FESEM micrographs of cross-sections of hematite photoanodes prepared with FeOOH powders synthesized with different levels of LA. (a) Fe_2O_3 (0g LA); (b) Fe_2O_3-FeO_x (0.1g LA); (c) Fe_2O_3-FeO_x (0.2g LA); (d) Fe_2O_3-FeO_x (0.3g LA); (e) Fe_2O_3-FeO_x (0.4g LA). Photoanodes were constructed using as a substrate aluminoborosilicate glass with conductive FTO layer.

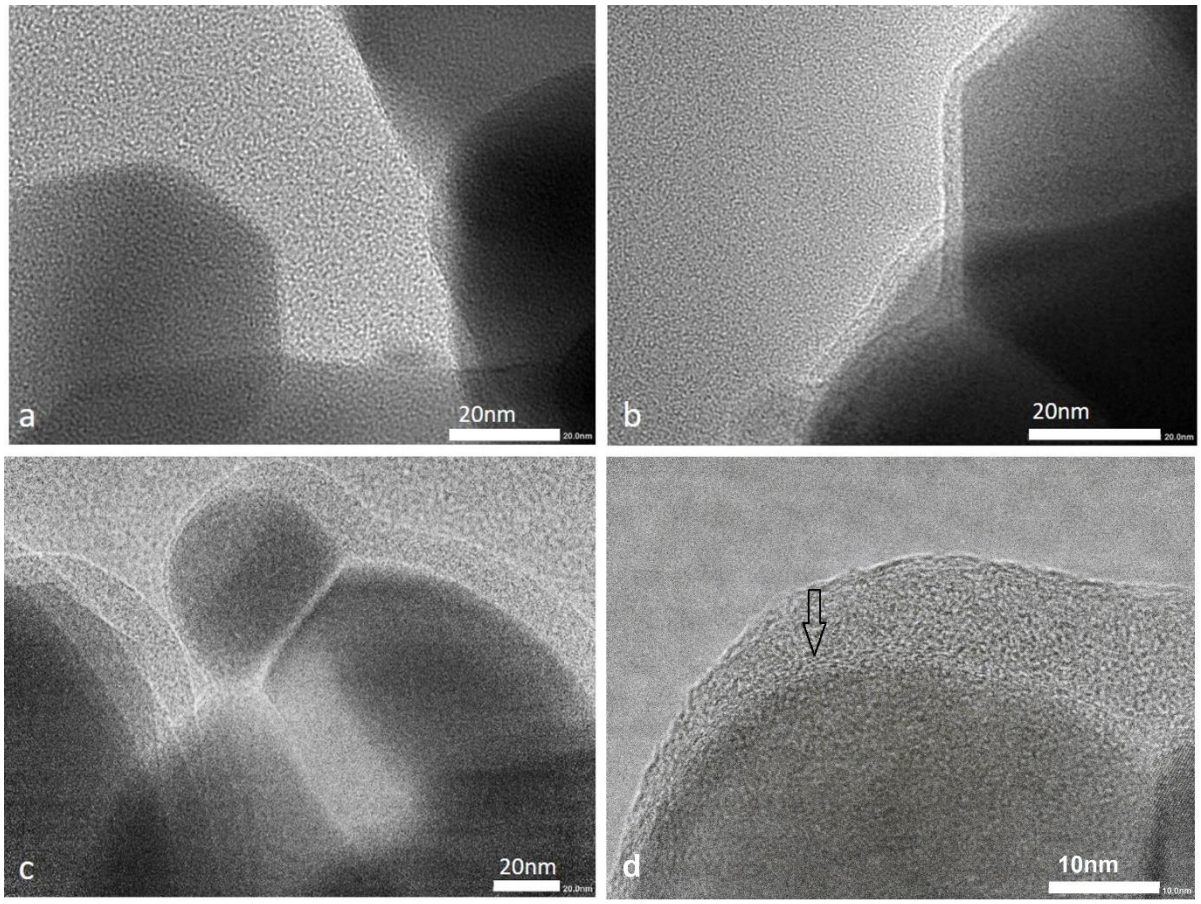

Figure S4. TEM micrographs of material scraped from hematite photoanodes prepared with FeOOH powders synthesized with different levels of LA. (a) Fe_2O_3 (0g LA); (b) Fe_2O_3-FeO_x (0.2g LA); and (c-d) Fe_2O_3-FeO_x (0.4g LA). Upon using LA in the synthesis procedure, hematite crystal surfaces are terminated with a coating of amorphous FeO_x material. Hematite lattice fringes were absent in this overlying amorphous layer. Occasional 2-3nm zones of graphitic carbon sheets between hematite and amorphous layer were also present (arrowed) in Fe_2O_3-FeO_x (0.4g LA) sample.[3]

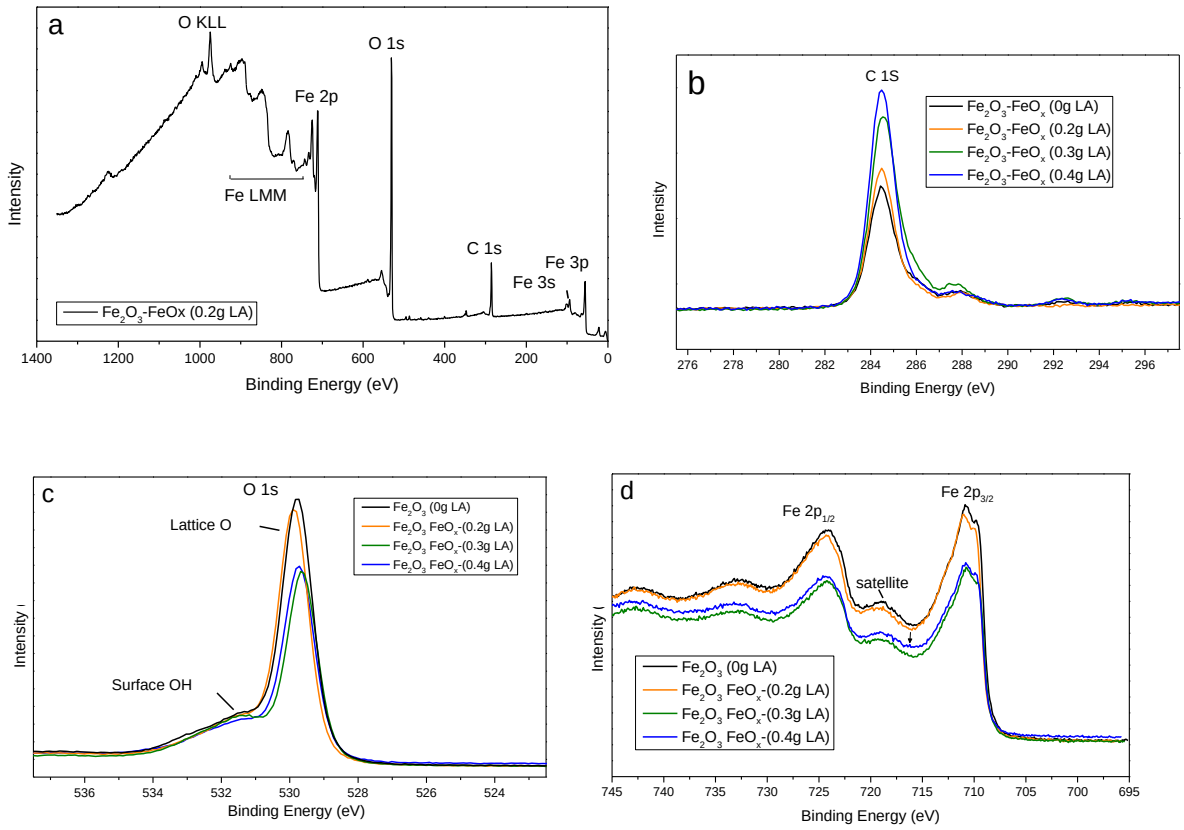

Figure S5. XPS analysis of hematite photoanodes prepared with FeOOH powders synthesized with different levels of LA. (a) Representative XPS survey of a hematite photoanode, Fe_2O_3-FeO_x (0.2g LA); (b) C 1s region with increasing intensities with increasing LA; (c) O1s region with increasing contribution of surface hydroxyl groups region with increasing LA; (d) Fe 2p region, where an arrow indicates a trace peak associated with Fe^{2+} content for the Fe_2O_3-FeO_x (0.4g LA) sample.[4]

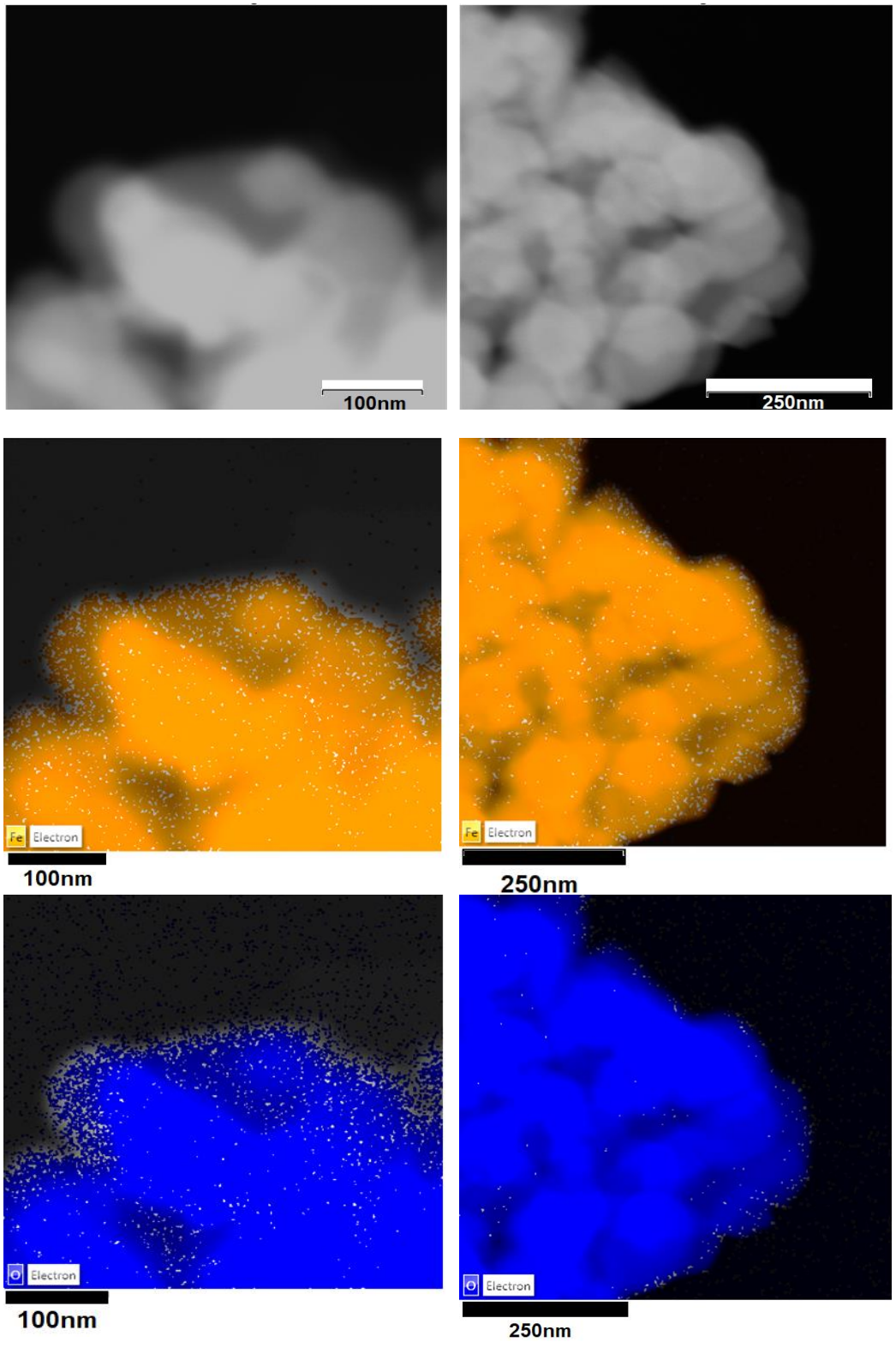

Figure S6. STEM EDX elemental mapping of material scraped from Fe_2O_3-FeO_x (0.4g LA) photoanode, showing Fe (orange) and O (blue). The coating layer regions gave emissions corresponding to iron (orange) and oxygen (blue) only, with all other elements at background levels.

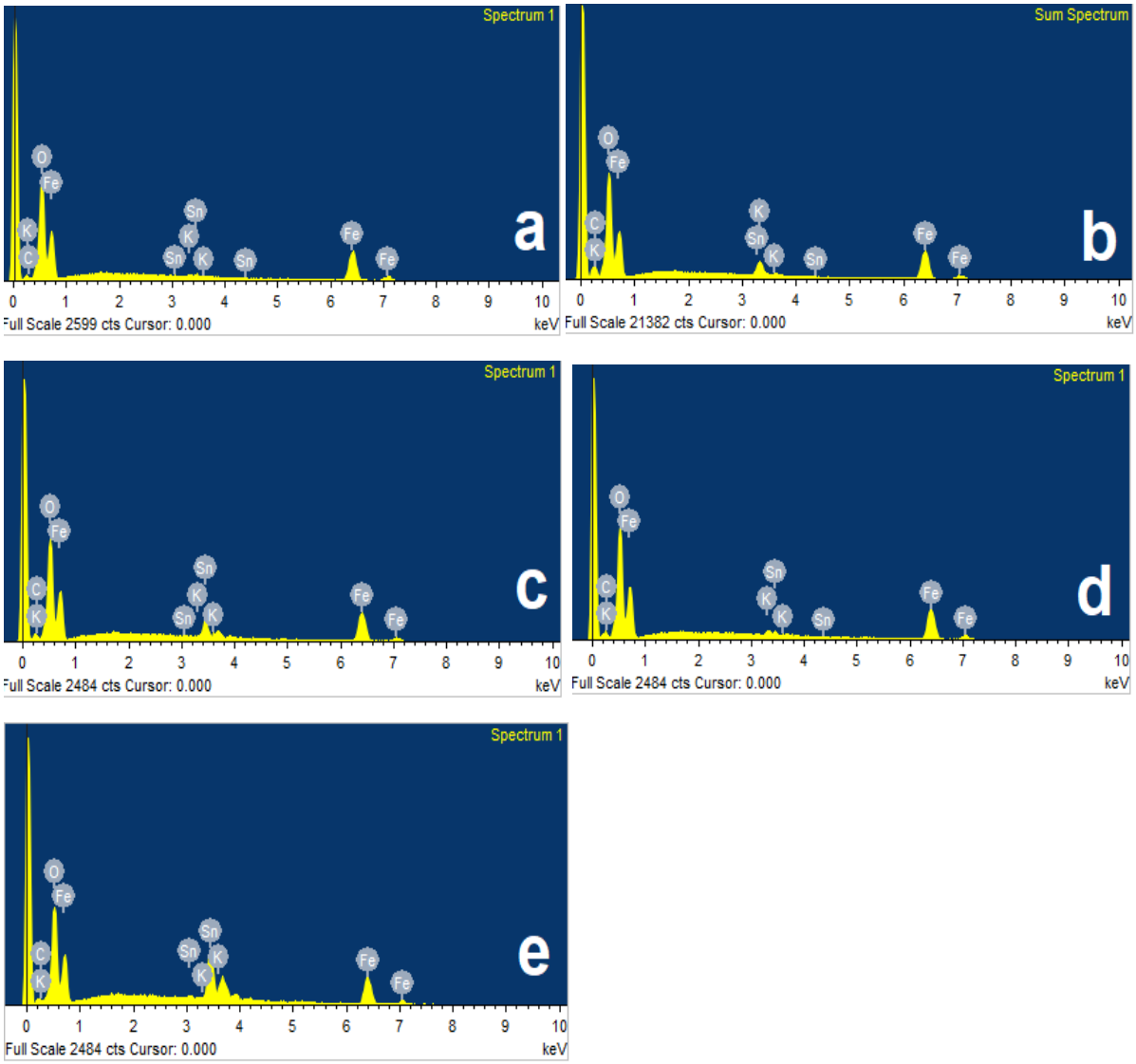

Figure S7. EDXS spectra obtained at low magnification SEM of hematite photoanodes prepared with FeOOH powders synthesized with different levels of LA. (a) Fe_2O_3 (0g LA); (b) Fe_2O_3-FeO_x (0.1g LA); (c) Fe_2O_3-FeO_x (0.2g LA); (d) Fe_2O_3-FeO_x (0.3g LA); and (e) Fe_2O_3-FeO_x (0.4g LA).

Table S2. EDXS analysis of elemental composition (for elements of atomic weight > N) of hematite photoanodes prepared with FeOOH powders synthesized with different levels of LA.

	Fe_2O_3 (0g LA)		Fe_2O_3-FeO_x (0.1g)		Fe_2O_3-FeO_x (0.2g)		Fe_2O_3-FeO_x (0.3g)		Fe_2O_3-FeO_x (0.4g)	
Element	Wt %	At %	Wt %	At %	Wt %	At %	Wt%	At%	Wt%	At%
O K	27.43	57.40	27.45	56.69	26.04	58.51	27.38	57.60	22.22	57.27
K K	0.49	0.42	6.67	5.64	0.00	0.00	2.18	1.88	0.00	0.00
Fe L	68.83	41.26	61.72	36.52	56.03	36.06	64.40	38.81	40.22	29.69
Sn L	3.24	0.91	4.16	1.16	17.93	5.43	6.04	1.71	37.56	13.04

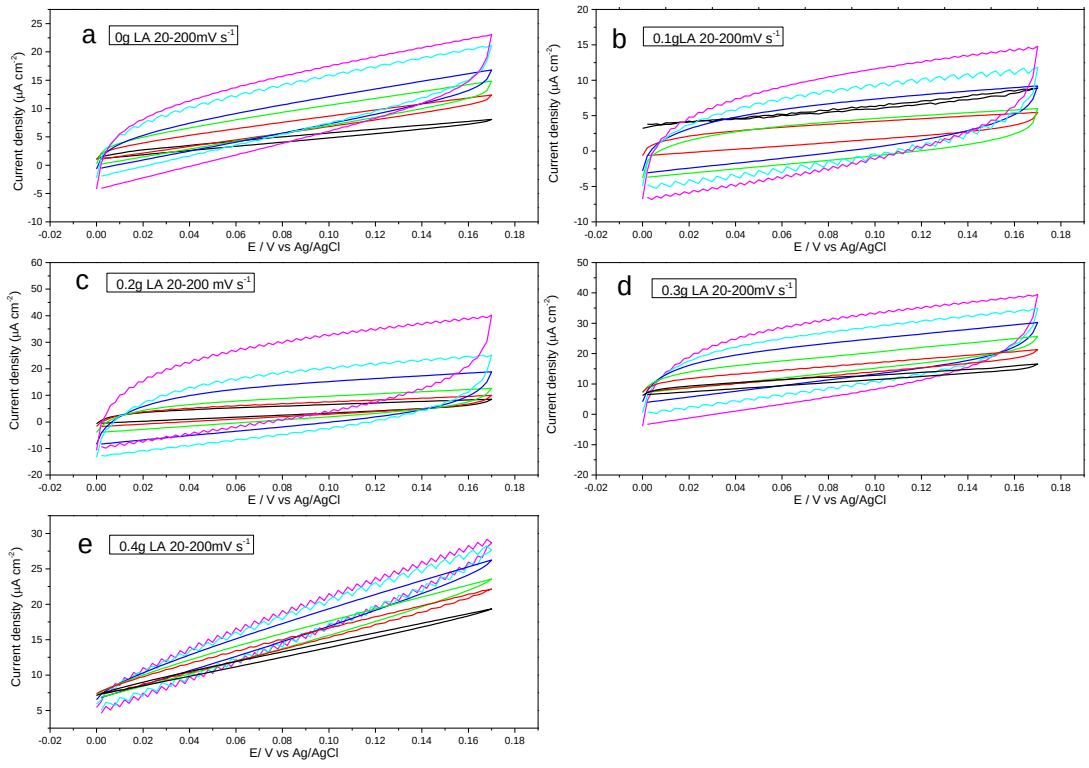

Fig S8. Cyclic voltammetry curves of hematite photoanodes prepared with FeOOH powders synthesized with different levels of LA. (a) Fe_2O_3 (0g LA); (b) Fe_2O_3-FeO_x (0.1g LA); (c) Fe_2O_3-FeO_x (0.2g LA); (d) Fe_2O_3-FeO_x (0.3g LA); and (e) Fe_2O_3-FeO_x (0.4g LA). Curves were measured at 20 (black), 30 (red), 50 (green), 100 (blue), 150 (cyan) and 200 (magenta) mV s^{-1} at applied potential of 0 to 0.17$V_{Ag/AgCl}$.

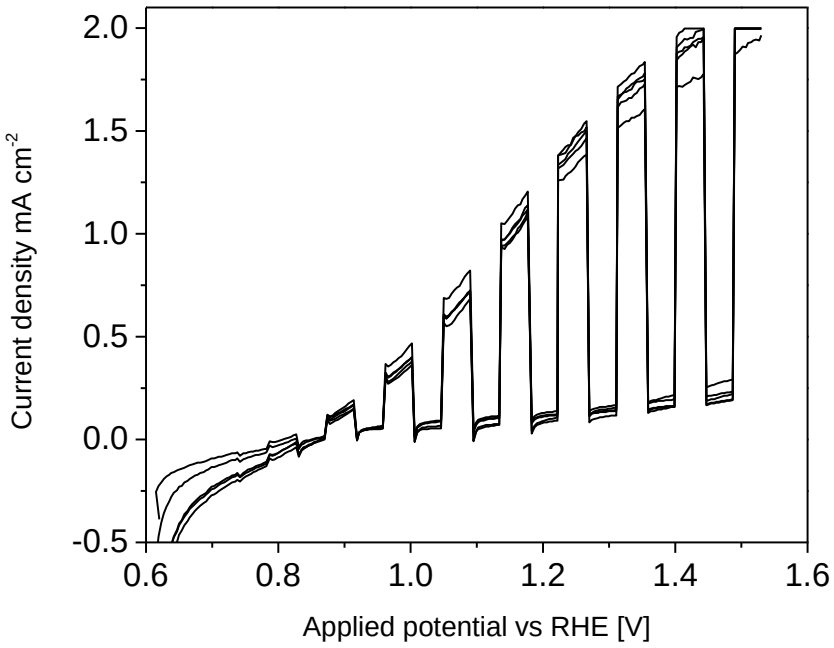

Figure S9. Photocurrent for five Fe_2O_3-FeO_x (0.2g LA) photoanode slides at different applied potentials. Measurements were made using 1M KOH as electrolyte under simulated sunlight (AM1.5G, 100mW cm^{-2}).

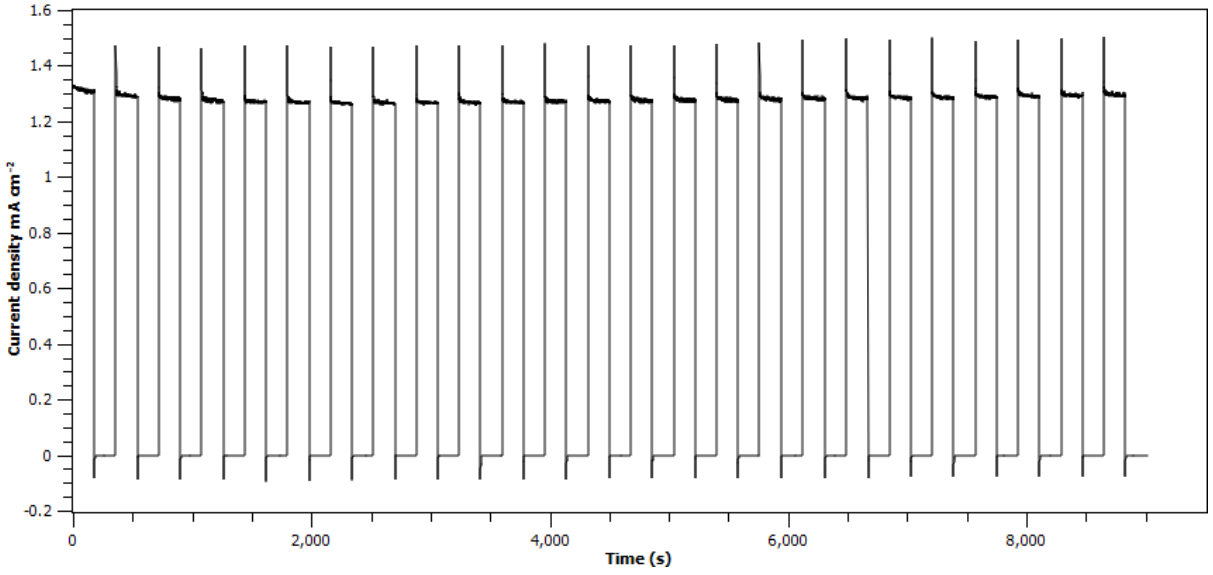

Figure S10. Current density of Fe_2O_3-FeO_x (0.2g) photoanode slide, over 2.5 h, conducted with chopped simulated sunlight (100mW cm^{-2}, AM1.5G filtered) in 1 M KOH at an applied potential $1.23V_{RHE}$.

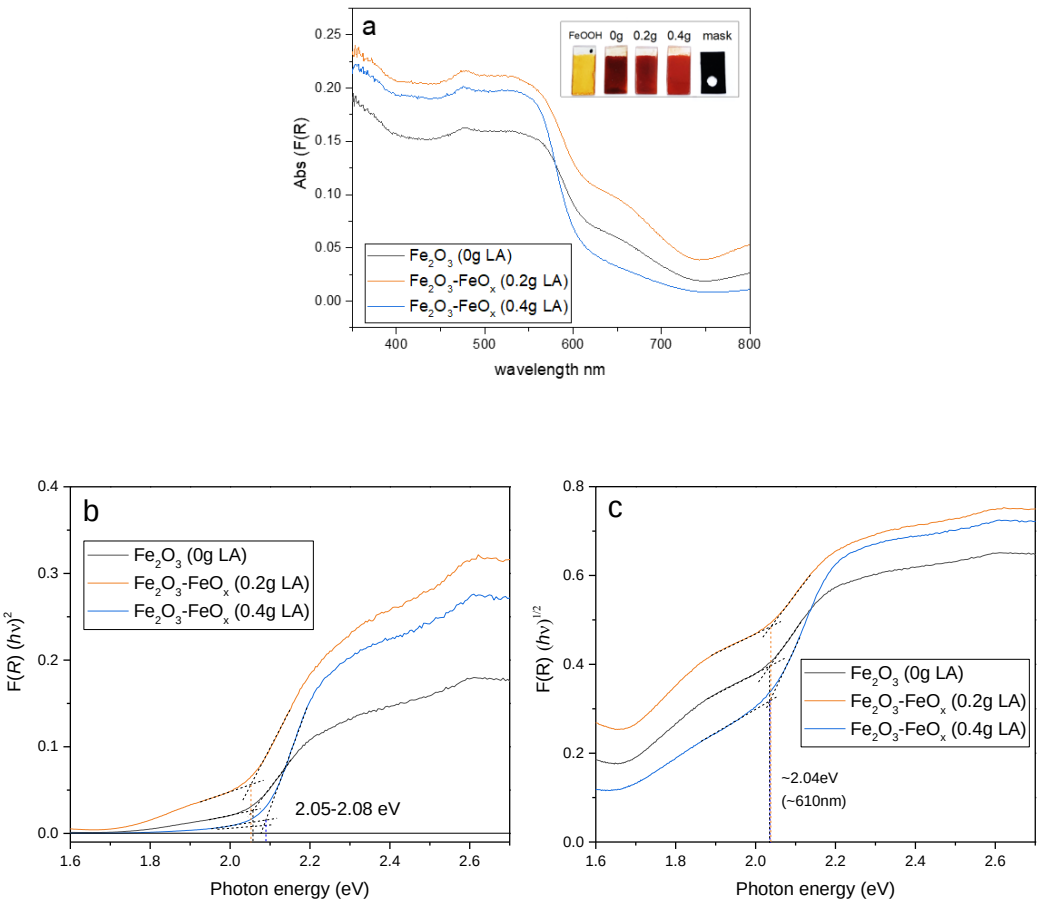

Fig S11. (a) UV-visible light $(F(R).hv)^n$) diffuse reflectance absorbance of hematite photoanodes prepared with FeOOH powders synthesized with different levels of LA (0, 0.2 and 0.4 g LA). Inset in (a) shows an as-deposited photoanode (labelled FeOOH) and photoanodes after heating to 800°C for 20 min (labelled 0 g, 0.2 g and 0.4 g, according to LA levels). The light shield mask with a circular aperture used to cover the hematite coating in PEC measurements is also shown; (b) Corresponding Tauc plot of $(hv)^2$ against photon energy showing direct band gaps of E_g 2.05-2.08 eV (605-596nm); (c) Corresponding Tauc plot of $(hv)^{1/2}$ against photon energy, showing indirect band gaps of E_g ~2.04 eV (608nm).

The Kubelka-Munk function, ***F(R)***, allows the optical absorbance of a sample to be approximated from its reflectance:

$$\mathbf{F(}\boldsymbol{R}\mathbf{)} = \frac{(1-R)^2}{2R}$$

For the hematite semiconductor samples Tauc plots of $(\boldsymbol{F(R)}.hv)^n$ vs hv are shown. The value of n is determined by the optical transition type, for the direct band gap $n = 2$ and for indirect $n = 1/2$. Intercepts of the straight line around the absorption edge region gives the optical band gaps.[5]

Measurement of oxygen evolution from photoanode

A custom-made 110ml square quartz cell with PFTE lid and air-tight ports for sample, Pt counter, reference electrode and N_2 bubble line was used. An O_2 sensor probe was used to measure O_2 evolution from the hematite photoanode. The sensor probe was a Pyroscience Firesting O2 sensor housed in a robust tip, coupled with a temperature probe for continuous temperature compensation. The probe tip houses a fluorescent dye that fluoresces relative to O_2 presence on brief flash illumination. The sample photoanode, Pt counter and Ag/ AgCl reference electrode were placed in 1 M KOH electrolyte and air-tight sealed in the chamber lid. The chamber electrolyte and headspace were flushed with N_2 for 30 min before the photoanode (0.55cm^{-2} exposed area) at an applied potential of 1.23V vs RHE was illuminated at 100 mW cm^{-2} for 1 hour. Evolution of O_2 was continuously monitored with the Pyroscience probe and the O_2 generation rate used to calculate Faradaic efficiency. The best performing Fe_2O_3-FeO_x (0.2g LA) and the Fe_2O_3 (0g LA) photoanodes were tested. However, the α-Fe_2O_3 (0g LA) photoanode generated poor O_2 evolution which was difficult to quantify, so results are not presented.

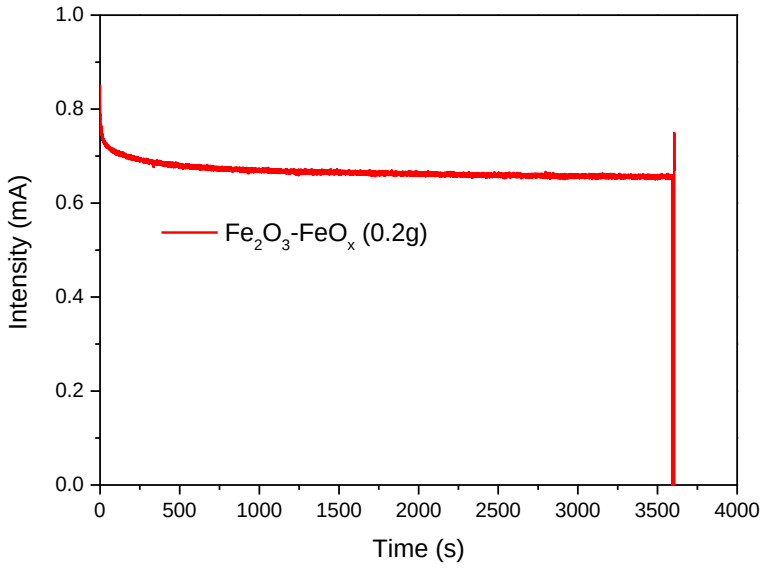

Figure S12. Current of Fe_2O_3-FeO_x (0.2g) photoanode slide over 1h, conducted with continuous simulated sunlight (100mW cm^{-2}, AM1.5G filtered) in 1 M KOH at an applied potential 1.23V_{RHE}. O_2 evolution was simultaneously monitored.

Faradaic efficiency calculation

To calculate the Faradaic efficiency, first the amount of O_2 evolved in the headspace of the PEC cell was calculated using the ideal gas law and measurements of the %O_2 and O_2 in the electrolyte solution was estimated using Henry's law and added to the measured values in the headspace.[6.7] Next, the

theoretical amount of O_2 expected for a water oxidation reaction with 100% Faradaic efficiency was calculated. The following equation (eq S1) was used:

$$Q=(e^{-})*F \qquad (S1)$$

where Q is the charge in C, obtained from the photocurrent-time curve; $n\ (e^{-})$ is the number of electrons in mol; and F is the Faraday constant (96485.3329 C mol^{-1}). The theoretical amount of O_2 generated was calculated by dividing $n\ (e^{-})$ by four, which is the number of electrons involved in the oxidation of water. Finally, the Faradaic efficiency was calculated by dividing the amount of O_2 evolved in the headspace by the theoretical amount of O_2 expected for 100% Faradaic efficiency (µmol / µmol x 100).

References

1. Lafuente B, Downs R T, Yang H, Stone N (2015) The power of databases: the RRUFF project. In: Highlights in Mineralogical Crystallography, T Armbruster and R M Danisi, eds. Berlin, Germany, W. De Gruyter, pp 1-30.
2. Xiao, F., Li, W., Fang, L., Wang, D., Synthesis of akageneite (beta-FeOOH)/reduced graphene oxide nanocomposites for oxidative decomposition of 2-chlorophenol by Fenton-like reaction. Journal of Hazardous Materials 2016, 308, 11-20.
3. Deng, J., Lv, X., Gao, J., Pu, A., Li, M., Sun, X. and Zhong, J., Facile synthesis of carbon-coated hematite nanostructures for solar water splitting. RSC Energy and Environmental Science, 2013, 6, 1965-1970.
4. Seabold, J.A. and Choi. K.S., Effect of a Cobalt-Based Oxygen Evolution Catalyst on the Stability and the Selectivity of Photo-Oxidation Reactions of a WO_3 Photoanode. Chem. Mater., 2011, 23, 1105–1112.
5. Zhebo Chen, Z., Dinh, H., Miller, E., UV-Vis Spectroscopy. In: Photoelectrochemical Water Splitting. SpringerBriefs in Energy. Chapter 5.4.; Springer, New York, NY (2013).
6. Lhermitte, C. R.; Garret Verwer, J.; Bartlett, B. M., Improving the stability and selectivity for the oxygen-evolution reaction on semiconducting WO3 photoelectrodes with a solid-state FeOOH catalyst. Journal of Materials Chemistry A 2016, 4 (8), 2960-2968
7. Jia, H.; Stark, J.; Zhou, L. Q.; Ling, C.; Sekito, T.; Markin, Z., Different catalytic behavior of amorphous and crystalline cobalt tungstate for electrochemical water oxidation. RSC Advances 2012, 2 (29), 10874-10881.